

The Impact of Measurement Conditions on Solar Cell Efficiency

Michael Rauer,* Andreas Fell, Wilkin Wöhler, David Hinken, Christian Reichel, Karsten Bothe, Martin C. Schubert, and Jochen Hohl-Ebinger

Precise solar cell measurements become more and more challenging due to the increasing complexity of metallization patterns and the sensitivity to rear side illumination for bifacial cell concepts. In this context, the measurement conditions under which conversion efficiencies are determined need to be closely examined: Different efficiency values can occur for the same solar cell because of different measurement conditions. To provide more transparency, a notation has recently been published, which unambiguously characterizes the measurement conditions used and which is included in the calibration documents of the calibration laboratories ISFH CalTeC and Fraunhofer ISE CalLab PV Cells. As this notation is held rather technical and no quantitative assessment is given so far, herein, the effects associated with different measurement conditions are analyzed and quantified in detail for typical industrial-type solar cells. It is shown that varying the measurement conditions as well as the busbar concept can lead to significant differences in measured efficiency of 0.5%_{abs}. The power gains coming from different cell measurement configurations do not occur in the same manner on the module level though and can lead to considerable variations in cell-to-module power factors. Several hints to increase the significance of solar cell measurements are given.

1. Introduction


In recent years, many technical innovations have been introduced into solar cell fabrication. Solar cells have become larger, and the number of busbars has increased significantly.^[1] At the same time the width of the busbars rapidly decreased and is nowadays hardly larger than the width of a grid finger.^[1] In

addition, solar cells have become bifacial and exhibit sensitivity to rear side illumination. All these innovations lead to an ongoing growth in solar cell conversion efficiency but at the same time make the precise measurement of the conversion efficiency more challenging and also ambiguous. Shrinking busbar widths lead to an increase of the potential distribution caused by the current flow along busbars, which makes the precise positioning of current and voltage sensing contacts increasingly critical.^[2] Furthermore, with the growing number of busbars, the increase in shading by the contacting system affects the measurement results more and more^[3,4] and requires the redesign of the contacting equipment. Additionally, for bifacial solar cells, the spectral reflectance of the measurement chuck becomes relevant as light can be transmitted through the cell, be reflected at the chuck surface, and re-enter the cell from the rear side.^[5–7]

Given these challenges for precise measurements, the conditions under which efficiency values are measured need to be closely examined. As a first step toward more transparency, an appendix to a recent version of the renowned Solar Cell Efficiency Tables of Progress in Photovoltaics has been published.^[8] An unambiguous notation for measurement conditions has been proposed in the appendix and new record entries to the Solar Cell Efficiency Tables will always be labeled accordingly. A drawback of the universality of the notation is its technical character, which can complicate understanding and interpretation of the results. In this article, we therefore focus on explaining the notation and quantifying the effect of measurement conditions based on well-comprehensible simulations as well as measurements. The significance of the measurement conditions is analyzed by evaluating the prediction of the later module performance by solar cell measurements.

M. Rauer, A. Fell, W. Wöhler, C. Reichel, M. C. Schubert, J. Hohl-Ebinger
Photovoltaics
Fraunhofer Institute for Solar Energy Systems (ISE)
Heidenhofstraße 2, 79110 Freiburg, Germany
E-mail: michael.rauer@ise.fraunhofer.de

D. Hinken, K. Bothe
Photovoltaics
Institute for Solar Energy Research Hamelin (ISFH)
Am Ohrberg 1, 31860 Emmerthal, Germany

 The ORCID identification number(s) for the author(s) of this article can be found under <https://doi.org/10.1002/solr.202300873>.

© 2023 The Authors. Solar RRL published by Wiley-VCH GmbH. This is an open access article under the terms of the Creative Commons Attribution-NonCommercial-NoDerivs License, which permits use and distribution in any medium, provided the original work is properly cited, the use is non-commercial and no modifications or adaptations are made.

DOI: 10.1002/solr.202300873

2. Notation for Measurement Conditions

The notation proposed to the Solar Cell Efficiency Tables distinguishes different options for front and rear contacting as well as different chuck reflectance. In the following, the notation is briefly introduced and then explained on typical measurement configurations.

2.1. Introduction to Notation

2.1.1. Contacting Options

For solar cells with busbars, the electrical contacts are generally applied to the busbars and the finger grid is not contacted. Although not yet specified in international standards, there is a consensus that the electrical contacts thereby should be established along the entire length of the busbars. This represents module integration with an ideal, well-conductive interconnector. Therefore, only the finger but not the busbar resistance contributes to the overall series resistance. This contacting scheme is denoted as *busbar-resistance neglecting (brn)* configuration. As the series resistance of the finger grid depends on the length of the fingers, the number of busbar has to be specified. The brn configuration is conformal with international IEC standards.^[9,10]

For busbarless solar cells, more advanced contacting options are commonly required. By applying a high number of current contacts or by advanced voltage sensing,^[11,12] a contact to the entire grid including fingers can be emulated. As the series resistance of the finger grid does not contribute in this contacting scheme, it is denoted as *grid-resistance neglecting (grn)* configuration.

Further contacting options exist for busbarless cells^[13–15]: By applying electrical contacts locally to the grid of solar cells, the grid resistance can also be included in the measurement. This scheme is denoted as *grid-resistance including (gri)* configuration. The number of current contacts has to be specified here. Although this contacting option is important for correctly describing the module application of the solar cells,^[3] it is currently difficult to realize correctly and is rarely requested in calibration laboratories. Therefore, it has not been considered in this study.

All contacting configurations have in common that the shading of the contacting system is eliminated for the measurements by increasing the irradiance in the illuminated area to compensate for the shaded area. This has comparability reasons: The extent of shading by the contacting system depends on the solar simulator divergence and the dimensions of the contacting system. Thus, it can differ between different laboratories. By elimination of shading, it is ensured that similar currents can be measured at different facilities. It needs to be considered here that high extents of shading by the contacting system can also affect the measured fill factor (FF).^[3,4]

The contacting configurations mentioned above can be used to contact the front and the rear sides of bifacial solar cells, which are the most commonly produced type of solar cells.^[1] Further contacting options exist for monofacial solar cells with fully metallized rear sides, which are not considered in this study though. For more details, please refer to ref. [8].

2.1.2. Chuck Reflectance

Chuck reflectance becomes relevant for bifacial solar cells as light of long wavelengths can be transmitted through the solar cell, be reflected at the measurement chuck, and can thus contribute to the current of the solar cell.^[5–7] The notation proposed to the Solar Cell Efficiency Tables distinguishes between two chuck types commonly used in calibration laboratories: Chucks with spectral reflectance values $R_{>900\text{ nm}}$ below 15% in the relevant wavelength range above 900 nm are denoted as *nonreflective chuck (nrc)*, and chucks with $R_{>900\text{ nm}}$ above 85% are denoted as *highly reflective chuck (hrc)*. Although the IEC technical specification 60904-1-2 suggests using nonreflective chucks,^[10] the application of reflective chucks can be reasonable for certain module layouts. This will be further investigated in Section 4.

2.2. Measurement Configurations

Several representative measurement configurations have been considered in this study, which are shown schematically in **Figure 1**. These configurations are briefly introduced in the following, and the corresponding notation is explained.

(1) Baseline Configuration (brn | brn, nrc)

As first configuration, contact bars are applied to the solar cell as front contact and a lowly reflective and nonconductive measurement chuck with embedded electrical contacts is used as rear contact. A temporary electrical contact is thus established to all front and rear busbars, so that the front and rear contacting scheme is a busbar-resistance neglecting (brn) scheme. For completely describing the contacting scheme, the busbar number needs to be specified.

The spectral reflectance of a black chuck as it is typically used in calibration laboratories is shown in **Figure 2**. As the reflectance in the wavelength range above 900 nm is 6.5% in average, the rear contact is additionally classified as nonreflective chuck (nrc). From a normative point of view, this measurement

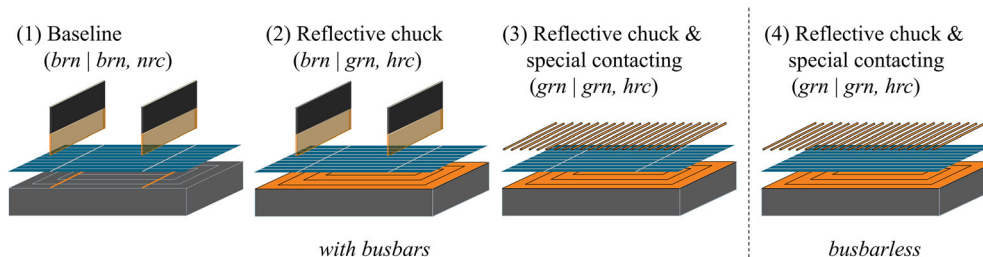


Figure 1. Representative measurement configurations used for the quantitative evaluation. Details on the different configurations and the corresponding notation are given in Section 2.2.

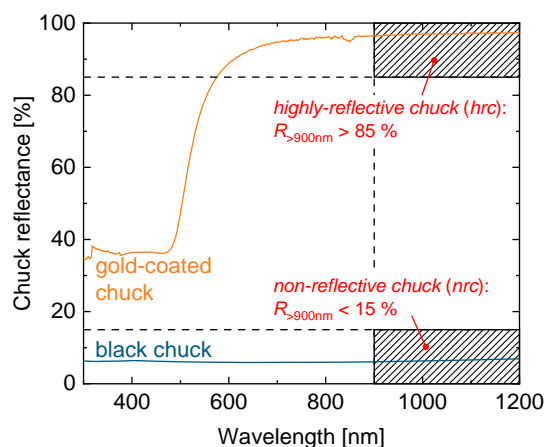


Figure 2. Spectral reflectance of a black (blue line) and a metal chuck (orange line) as they are typically used in calibration laboratories. For reflectance values $R_{>900\text{ nm}}$ in the wavelength range larger than 900 nm, which is relevant for transmittance of light through Si solar cells, the rear contacts are denoted as *nonreflective chuck (nrc)* for $R_{>900\text{ nm}} < 15\%$ or as *highly reflective chuck (hrc)* for $R_{>900\text{ nm}} > 85\%$.

configuration should be used to be compliant with international IEC standards. Moreover, this measurement configuration is comparable to measurement conditions in production lines, where contact bars are used as front and rear contacts, provided that an appropriate reference cell has been used for the calibration of the solar simulator.

(2) Reflective Chuck Configuration (brn | grn, hrc)

For the second configuration, the front contacting method has been kept identical and a brn scheme has been used as front contact. The rear contact however is changed to a metalized chuck. As the surface of the chuck is conductive, the entire rear grid including fingers and busbars is contacted, so that the rear contacting scheme is a grid-resistance neglecting (grn) scheme. The spectral reflectance of a gold-coated chuck as it is often used in calibration laboratories is approximately 95% in average in the relevant wavelength range, as shown in Figure 2. The rear contact is therefore additionally classified as highly reflective chuck (hrc). The reflective-chuck measurement configuration has historically been developed for monofacial solar cells with fully metalized rear contact but is still often used in research-and-development environments for bifacial solar cells as it is compatible with a variety of different rear side metallization concepts.

(3) Reflective Chuck and Special Contacting Configuration (grn | grn, hrc)

For the third configuration, the front contacting scheme has been changed to a special contacting option that is commonly used for busbarless solar cells. By applying a high number of current contacts or by adapted voltage sensing, a contact to the entire front grid including fingers and busbars can be emulated, which leads to the neglecting of the front grid series resistance. The front

contacting scheme is therefore a grid-resistance neglecting (grn) scheme. Although this contacting method has been developed for busbarless solar cells, it can in principle also be applied to solar cells with busbars and is becoming increasingly attractive as front busbar patterns are becoming more and more complex. Calibration laboratories refrain from using it for busbar-based cells though, because it is not in agreement with IEC standard 60904-1 and is in contradiction to the intended use of the solar cell in the module.

(4) Reflective Chuck, Special Contacting, and Busbarless (grn | grn, hrc)

As a fourth configuration, it has been assumed that the busbar print has been omitted and a busbarless solar cell layout is considered. Except the missing busbars, the solar cell has not been changed and thus exhibits similar cell physics. A grid-resistance neglecting (grn) front contact scheme is therefore applied, which is commonly used for busbarless solar cells.^[11] Although this configuration seems like a disruptive one as the solar cell itself has been changed, it is important to consider busbarless concepts, as busbarless concepts compete with busbar-based concepts and need to be compared objectively.

3. Influence of Measurement Conditions on Solar Cell Conversion Efficiency

3.1. Solar Cell Model

To representatively quantify the influence of the measurement conditions on the current-voltage (I - V) parameters, bifacial industrial-type passivated-emitter-and-rear-cell (PERC) and tunnel-oxide-passivated-contact (TOPCon) solar cell concepts have been modeled using Quokka3.^[16] A typical M10 half-cell format^[1] has been used for both concepts. The optical characteristics have thereby been adapted to measured data of comparable cells. **Figure 3** shows the external quantum efficiency (EQE) and

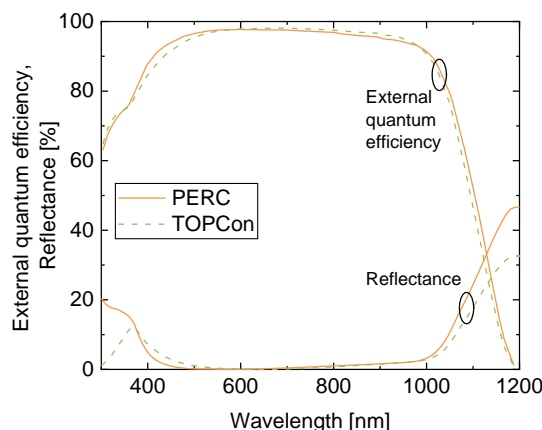


Figure 3. EQE and spectral reflectance of PERC (solid, orange lines) and TOPCon (dashed, green lines) solar cells. The reflectance curves are thereby corrected for reflection by fingers and busbars as Quokka3 accounts for metallization reflection separately.

Table 1. Parameters of the Basore model for PERC and TOPCon solar cells. R_{o-1} parameterizes the first internal reflection, R_f all subsequent internal reflections at the front, R_r all subsequent internal reflections at the rear, and A_{ppp} the parasitic absorption at the rear.

	R_{o-1}	R_f	R_r	A_{ppp}
PERC	0.9648	0.9054	0.9418	0.0068
TOPCon	0.9179	0.9329	0.9472	0.0095

spectral reflectance curves for the PERC and TOPCon solar cells. The parameters of the Basore model, which characterize the internal light-trapping behavior, are summarized in **Table 1** for both solar cell types. For correctly considering the specular and diffuse chuck reflectance, a recently developed extension^[17] of the light trapping model of Rand and Basore^[18,19] has additionally been used. The extended model has been calibrated to measured reflectance and transmission data.

Further and more specific details on the cell models are given in the following. The electrical parameters are based on literature^[1] and empirical data for recent industrial cells.

3.1.1. Bifacial PERC Solar Cell

As base material, p-type silicon with a resistivity of $0.8 \Omega\text{cm}$ and a thickness of $155 \mu\text{m}$ has been used. To model recombination in the base, an interstitial iron concentration of $7 \times 10^9 \text{cm}^{-3}$ has been assumed in addition to intrinsic radiative and Auger recombination.

On the front, a selective n^+ emitter with a sheet resistance of $155 \Omega\text{sq}^{-1}$ and a saturation current density of 22fA cm^{-2} has been applied between the contacts. The front finger width has been set to $24.6 \mu\text{m}$ and the finger distance to 1.2mm , and a front grid resistivity of $19.8 \text{m}\Omega\text{cm}^{-1}$ has been used. The front contact resistivity has been set to $1 \text{m}\Omega\text{cm}^2$.

On the rear, a passivation layer stack of aluminum oxide and silicon nitride with a saturation current density of 5fA cm^{-2} has been used. The contact opening of the rear fingers has been set to $50 \mu\text{m}$ with a saturation current density of 248fA cm^{-2} and a total finger width of $143 \mu\text{m}$. A rear finger pitch of 1mm , a rear contact resistivity of $4.5 \text{m}\Omega\text{cm}^2$, and a rear grid resistivity of $7.2 \text{m}\Omega\text{cm}^{-1}$ have been used.

Ten busbars with front and rear widths of 95 and $1065 \mu\text{m}$, respectively, have been assumed, which are not in direct electrical contact to the emitter. 7 busbar pads with an average dimension of $1.1 \times 0.9 \text{mm}^2$ have been used on the front and 4 busbar pads with a dimension of $5 \times 1.3 \text{mm}^2$ on the rear.

Table 2. Simulated current–voltage (I – V) parameters and bifaciality in conversion efficiency of industrial-type PERC and TOPCon solar cells using a baseline measurement configuration.

	Short-circuit current density J_{sc} [mA cm^{-2}]	Open-circuit voltage V_{oc} [mV]	FF [%]	Conversion efficiency η [%]	Bifaciality in η [%]
PERC	40.7	694	82.1	23.2	71.3
TOPCon	40.5	717	83.0	24.1	78.4

3.1.2. Bifacial TOPCon Solar Cell

n-type Si with a resistivity of $1.1 \Omega\text{cm}$, a thickness of $150 \mu\text{m}$, and a fixed low-injection minority carrier lifetime of 5ms have been used as base material.

A homogenous p^+ emitter exhibiting a sheet resistance of $120 \Omega\text{sq}^{-1}$ and a saturation current density of 12fA cm^{-2} has been assumed on the front. The front finger width has been set to $31 \mu\text{m}$ with a pitch of 1.3mm , and a front grid resistivity of $30.5 \text{m}\Omega\text{cm}^{-1}$ has been applied. The front contact resistivity is $1.0 \text{m}\Omega\text{cm}^2$.

A tunnel-oxide-passivated n^+ rear with a sheet resistance of $160 \Omega\text{sq}^{-1}$ and a saturation current density of 5fA cm^{-2} has been used. A rear finger width of $40 \mu\text{m}$ with a pitch of 1.25mm has been assigned. This results in a rear grid resistivity of $19.2 \text{m}\Omega\text{cm}^{-1}$. The rear contact resistivity is set to $1.3 \text{m}\Omega\text{cm}^2$.

16 busbars with a front and rear width of 69 and $78 \mu\text{m}$, respectively, have been used. Six pads on front and rear with average dimensions of $1 \times 0.7 \text{mm}^2$ have been considered.

3.2. Simulation and Measurement Results

To quantify the effect of measurement configurations, the I – V parameters of the PERC and TOPCon solar cells have been simulated as they would be measured with the four different measurement configurations described in Section 2.2. **Table 2** shows the I – V results with the baseline configuration, which is the measurement configuration in accordance with international standards.

For the evaluation and visualization of the effect of the measurement conditions, the baseline configuration has been used as reference configuration and the difference in the efficiency value $\Delta\eta$ between the other measurement configurations and the baseline configuration has been calculated; see **Figure 4**. $\Delta\eta$ has thereby been split into short-circuit current density J_{sc} , open-circuit voltage V_{oc} , and FF contributions. The authors like to point out that these calculations need to be considered as example cases and that exact values may vary for other contacting geometries or different solar cell structures. The intention is to provide a relevant showcase to quantify the magnitude of these effects, which can be considered to be representative for similar cell designs.

3.2.1. Efficiency Difference for Configuration (2): Reflective Chuck

For the reflective-chuck configuration (2), there are two main effects leading to efficiency differences to the baseline configuration: As first effect, the contribution from light being

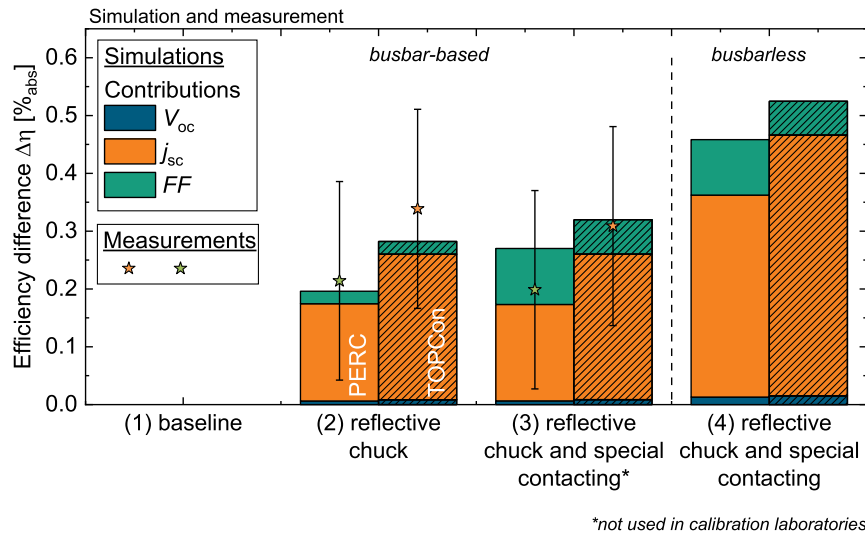


Figure 4. Simulated and measured efficiency difference $\Delta\eta$ between the baseline configuration and the other measurement configurations. The bars represent simulated values, which have additionally been split into J_{sc} , V_{oc} , and FF contributions. The stars show measured data on comparable solar cells. The measurement uncertainties (coverage factor of 2) thereby represent typical uncertainties for measurements with change in contacting system and similar calibration of the solar simulator. The authors want to point out that measurement configuration (3) is generally not used in calibration laboratories for measurements of solar cells with busbars.

additionally reflected at the surface of the reflective chuck leads to a minor increase in V_{oc} and a much larger increase in J_{sc} . This contribution is more pronounced for the TOPCon solar cell, as it features a higher spectral bifaciality in the long-wavelength range than the PERC solar cell. The difference in J_{sc} can also be seen in measurements of the EQE, see **Figure 5**. As second effect, the elimination of the series resistance of the rear contact finger grid results in a small $\Delta\eta$ increase caused by a higher FF. Although the rear grid resistivity is higher for the TOPCon than for the PERC cell, the corresponding series resistance is approximately similar because of the different numbers of busbars. The FF contributions are thus approximately identical for the two solar cell concepts.

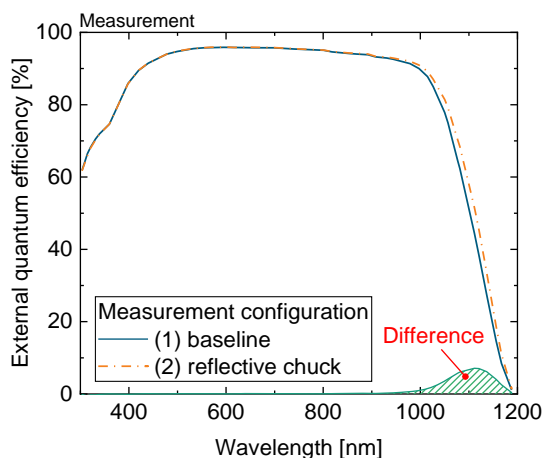


Figure 5. Measured EQE for the PERC solar cell with baseline (black, solid line) and reflective-chuck (orange, dash-dotted line) measurement configurations and resulting EQE difference (hatched area).

It is important to point out that optical effects (like the difference in chuck reflectance) and resistive effects (like the elimination of the rear grid resistance) are nearly independent from each other.

Strictly speaking, the bifacial solar cells cannot be regarded separately from the measurement system anymore: The devices under test are not simple “solar cells” but “solar cells on a black chuck” or “solar cells on a reflective chuck”, which means, in other words, that a certain chuck is required to realize such results with these solar cells.

The difference between the two measurement configurations also depends on the thickness of the solar cell. As it is expected that solar cells will become even thinner in the future,^[1] the impact of the cell thickness was additionally evaluated. **Figure 6** shows the $\Delta\eta$ values between baseline and reflective-chuck configurations as a function of the thickness of the solar cells. It can be seen that the J_{sc} contributions increase with decreasing cell thickness as more light is transmitted through the solar cells. The V_{oc} and FF contributions are only marginally affected. That means that the difference between the measurement configurations is expected to increase slightly in the future.

3.2.2. Efficiency Difference for Configuration (3): Reflective Chuck and Special Contacting

By changing the front contact to the special approach developed for busbarless solar cells, the efficiency difference $\Delta\eta$ to the baseline results increases further, see **Figure 4**. Optical contributions coming from the reflective chuck are similar to the reflective-chuck configuration (2), so that J_{sc} and V_{oc} contributions are nearly identical. Resistive effects differ, though, as the series resistance of the front finger grid is additionally eliminated. This leads to a further increase of the FF contribution, which is significantly larger

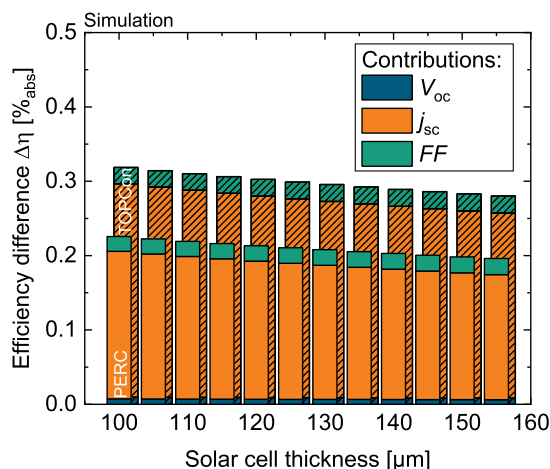


Figure 6. Simulated efficiency difference $\Delta\eta$ between baseline and reflective-chuck configuration as a function of the solar cell thickness for PERC (unshaded bars) and TOPCon solar cells (shaded bars). For visualization reasons, the bars are shown with a slight offset.

for the PERC than for the TOPCon solar cell. This difference is mainly caused by the different numbers of busbars.

To further illustrate this effect, the grid resistance and the busbar number of the PERC solar cell have been varied, as shown in **Figure 7**. $\Delta\eta$ is thereby approximately given by the FF difference because of negligible J_{sc} and V_{oc} differences. $\Delta\eta$ depends linearly on the grid resistance and with a $1/N_{BB}^2$ relation on the number N_{BB} of busbars.^[3] Therefore, higher busbar numbers tolerate much larger grid resistance values. Although the TOPCon solar cell exhibits a higher grid resistance, the effect on the efficiency is smaller for the TOPCon than for the PERC cell due the higher

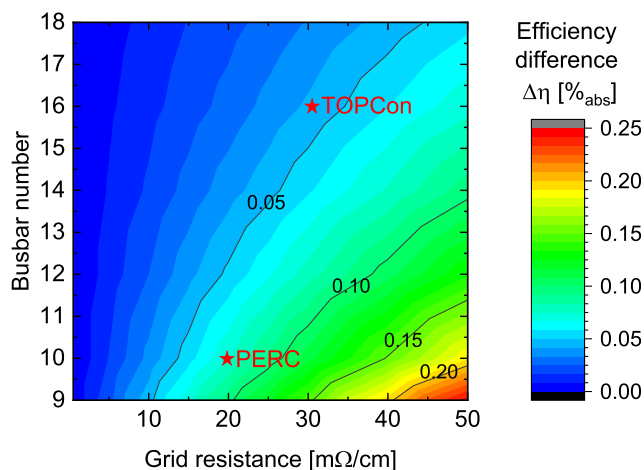


Figure 7. Simulated efficiency difference $\Delta\eta$ between reflective-chuck configuration (2) and reflective-chuck-and-special-contacting configuration (3) for a PERC solar cell as a function of the grid resistance and the busbar number. The grid resistance has been modified by varying the finger conductivity and keeping the finger pitch constant. Although the simulations are shown for the PERC cell here, they can be directly transferred to the TOPCon solar cell, as the absolute J_{sc} values of the PERC and TOPCon solar cells are comparable.

busbar number. In particular, for high busbar numbers, $\Delta\eta$ can become negligibly small, so that the busbar-resistance neglecting (brn) scheme is approximately similar to the grid-resistance neglecting (grn) contacting scheme. This is important for high-efficiency record devices, as will be discussed in Section 3.4.

Using measurement configuration (3), the PERC and TOPCon solar cell efficiencies are measured 0.3%_{abs} higher than using the baseline configuration. The authors again want to emphasize that measurement configuration (3) is generally not provided by calibration laboratories for busbar-based solar cells.

3.2.3. Efficiency Difference for Configuration (4): Reflective Chuck, Special Contacting, and Busbarless

Using the same measurement configuration on a busbarless solar cell layout, the contributions from the reflective chuck and from the special front contacting are nearly similar. In addition, there is a further efficiency increase of approximately 0.2%_{abs} for both PERC and TOPCon solar cells, see Figure 4. This is caused by the missing shading of the front busbars which leads to a significantly increased J_{sc} contribution. The J_{sc} increase is thereby nearly similar for the PERC and TOPCon solar cell as the higher busbar number of the TOPCon solar cell is compensated by a smaller busbar width and a reduced pad size. Using a busbarless solar cell concept and measurement configuration, the efficiency can thus be measured approximately 0.5%_{abs} higher for industrially relevant PERC and TOPCon solar cells.

3.3. Comparison of Simulations and Measurements

In addition to the simulation-based evaluation of measurement conditions presented in the previous section, I - V measurements of PERC and TOPCon solar cells with busbars have been carried out at ISFH CalTeC and Fraunhofer ISE CalLab PV Cells using different measurement configurations. Both calibration laboratories agreed very precisely.

For both baseline and the reflective-chuck measurement configurations, chucks with spectral reflectance as presented in Figure 2 have been used. Each of the front busbars has been contacted by an individual contact bar. For the rear contact, either the busbars or the entire rear grid have been contacted for the baseline and the reflective-chuck configuration, respectively. For measurements with the reflective-chuck-and-special-contacting configuration, the voltage sensing has been carried out between the busbars at the position of the average of the voltage distribution. This contacting scheme has only been used for this study and is generally not provided by calibration laboratories for solar cells with busbars. The solar cells used for the I - V measurements had a slightly lower efficiency level than the simulated ones, but comparable bifaciality and grid resistances, so that the measured differences in efficiency can be compared to the simulation results.

The stars in Figure 4 show the measured $\Delta\eta$ values. The error bars present typical measurement uncertainties which result from a change in the contacting system with similar calibration of the sun simulator. It can be seen that the measured $\Delta\eta$ values

agree very well with the simulation results within the measurement uncertainties.

3.4. Limitations of Notation

The notation for measurement conditions has been introduced as an important first step in creating transparency for measurement results. To keep the notation viable, its structure is as simple as possible. This inevitably entails limitations, which are briefly addressed in the following.

The busbar geometry strongly affects the efficiency differences between the brn and grn contacting schemes. Although the number of busbars is included in the notation, further quantities are not reported for simplicity. This can affect both resistive FF and optical J_{sc} differences.

Fill Factor Effects: The grid resistance, which is not explicitly specified in the notation, is needed to fully characterize the differences between the brn and grn contacting schemes, see Figure 7. Whereas for low busbar numbers, the FF difference depends significantly on the grid resistance, the FF difference is nearly independent from the grid resistance for higher busbar numbers. For solar cells with a high busbar number, the FF difference between the brn and grn contacting schemes can therefore become small. Please note that, for high grid resistances, high extents of shading by the contacting system can additionally reduce the measured FF.^[3,4]

J_{sc} Effects: To fully quantify the effect of busbar shading, the busbar widths and the solder pad dimensions need to be specified. In the sections presented above, industrially relevant busbar and pad dimensions have been considered. The extent of busbar shading can nevertheless differ for other metallization geometries: For solar cells with very thin busbars without solder pads, for example, busbar shading can be drastically reduced and the J_{sc} difference between a busbar-based and a busbarless concept can shrink strongly.

For solar cells with a high number of very thin busbars without solder pads, a busbar-based brn contacting scheme can therefore come close to a busbarless grn scheme, both in resistive and in optical terms. Even though the solar cell exhibits busbars, it resembles more a busbarless solar cell. This can be the case for record-type solar cells with busbars aiming at highest efficiency values, which commonly differ from industrial-type solar cells in terms of fabrication processes and metallization patterns.^[20] Record-type busbarless solar cells on the other hand can be fabricated with very low finger grid shading.

This discussion shows that the specification and interpretation of measurement configurations can be complex. To fully characterize the measurement conditions, the notation should be supplemented by the busbar widths and solder pad dimensions, the front and rear grid resistances as well as the spectral bifaciality of the solar cell in the long-wavelength regime. This is not feasible though.

4. Influence of Measurement Conditions on Cell-to-Module (CTM) Factors

In view of the different measurement configurations, the important question arises as to which of them is significant. According to the authors of this study, “significance” is defined by the quality of predicting the later module power with the solar cell measurements. This means that solar cell measurements should give an indication on the later performance of the solar cells in the modules and should enable an optimization of the solar cell for module implementation. Therefore, the module integration of the solar cells has been investigated in detail with cell-to-module (CTM) analyses^[21,22] by means of simulations using the sophisticated software SmartCalc.Module.^[23,24]

4.1. Modeling Module Implementation

Three different state-of-the-art module layouts^[1] have been evaluated for both PERC and TOPCon modules, see **Figure 8**: (i) a monofacial module layout with a glass front and a black-backsheet rear, (ii) a second monofacial layout with a glass front and white-backsheet rear, and (iii) a bifacial layout with a glass front and a glass rear.

Typical module dimensions have been used: 144 half-cut M10 solar cells interconnected in six strings in butterfly layout. Low-iron glass with antireflection coating and thickness of 3.2 mm have been assumed at the front of the two monofacial layouts (i) and (ii), and glass with a reduced glass thickness of 2.0 mm on front and rear for the bifacial layout (iii).

Ethylene vinyl acetate (EVA) or polyolefin elastomer (POE) encapsulants with a thickness of 0.45 mm have been used for the PERC and the TOPCon modules, respectively. For the cell interconnection, 10 round wires with a diameter of 270 μm have been applied for the PERC solar cells, and 16 round wires with a diameter of 250 μm have been applied for the TOPCon solar cells. Similar interconnector numbers have been used for

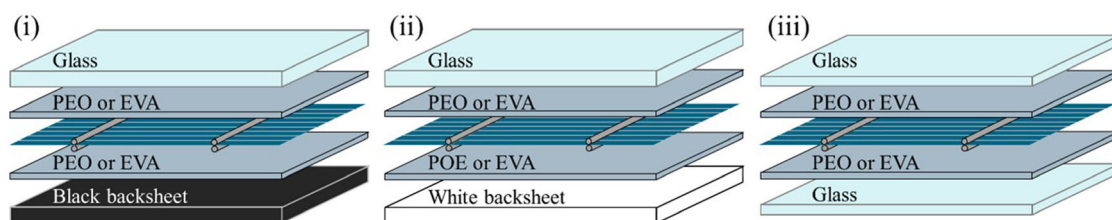


Figure 8. Module layouts used for evaluating the significance of measurement configurations. Details on the module specifications are given in Section 4.1.

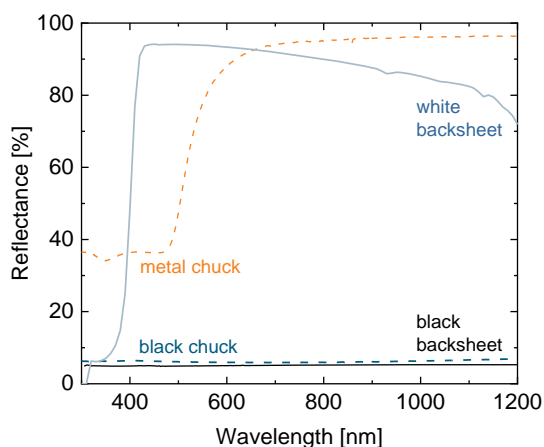


Figure 9. Spectral reflectance of the black (solid, black line) and white backsheet (solid, blue line) used for the calculation of the module powers in SmartCalc.Module. For comparison, the spectral reflectance of the black (dashed, blue line) and the metal chucks (dashed, orange line) are also shown.

busbar-based and busbarless solar cells because also similar grid resistances have been assumed.

The reflectance curves of the black and white backsheets are shown in **Figure 9**. The bifacial glass–glass module transmits all the light through the module, so that the spectral reflectance is effectively zero. The spectral reflectance of the black backsheet and of the bifacial layout is therefore similar to that of the black chuck. The reflectance of the white backsheet is comparable to that of the metal chuck in the relevant wavelength range above 900 nm, with some limitations though.

The module powers have been modeled for PERC and TOPCon modules for each of the three module layouts. The solar cell input parameters were taken from Quokka3 simulations, thereby assuming zero rear-side contributions as those are considered directly by SmartCalc.Module.

4.2. Results of Module Simulations

The simulated module powers for the three layouts are shown in **Figure 10** for solar cells with and without busbars. For purpose of clarity, only PERC module results are presented and discussed in the following. TOPCon modules yield comparable results.

The power of the PERC modules is nearly constant when interconnecting busbar-based and busbarless solar cells in the given module layout. In contrast, the sum of the solar cell power, which reflects the measured solar cell efficiency, depends significantly on the busbar design as well as on the measurement conditions. It can be seen that the power gains coming from different cell measurement configurations do not occur in the same manner in the module.

For further evaluation of the significance of measurement configurations, the cell-to-module power factors CTM_P were calculated.

$$CTM_P = \frac{P_{\text{module}}}{\sum P_{\text{cell}}} \quad (1)$$

The CTM_P factors strongly depend on the solar cell measurement configuration, as shown in **Figure 11**: The CTM_P factors and the sum of the cell powers are particularly anti-correlated as a direct consequence of the constant module powers. This means that choosing measurement conditions, which result in higher solar cell powers and efficiencies, leads to lower CTM_P factors. High solar cell efficiencies are then measured at the cost of low CTM_P values. Inappropriate solar cell measurement conditions can thus result in the overestimation of module performance when the CTM_P losses due to interconnection of the solar cells in the module layout are not considered. Hence, busbarless solar cell technologies in particular are at risk of incorrectly assessing the later module power. This has also been found by other research groups.^[25]

Although the relative CTM_P trends for the three different module layouts are similar, the absolute CTM_P values are shifted as the module powers differ. This means that similar CTM_P values are realized with other cell measurement configurations:

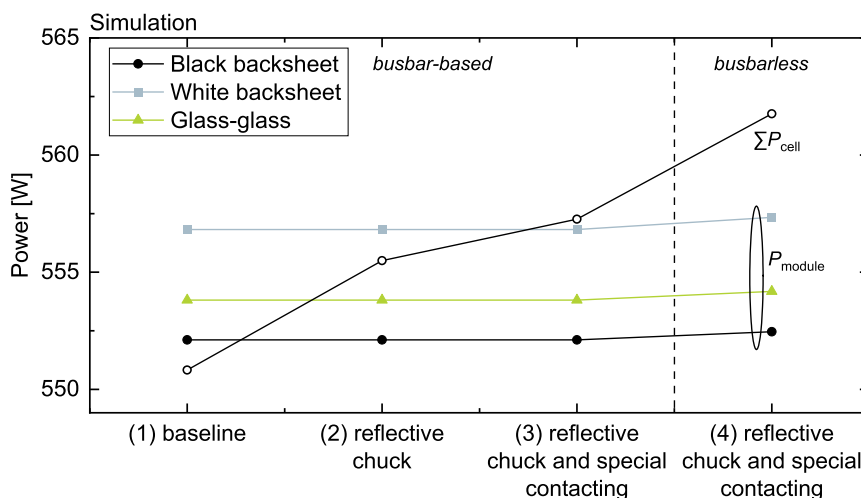


Figure 10. Simulated module power P_{module} for the three module layouts (closed symbols) and sum of the solar cell power $\sum P_{\text{cell}}$ (open symbols) as measured with the corresponding measurement configurations. For purpose of clarity, only the PERC results are shown here.

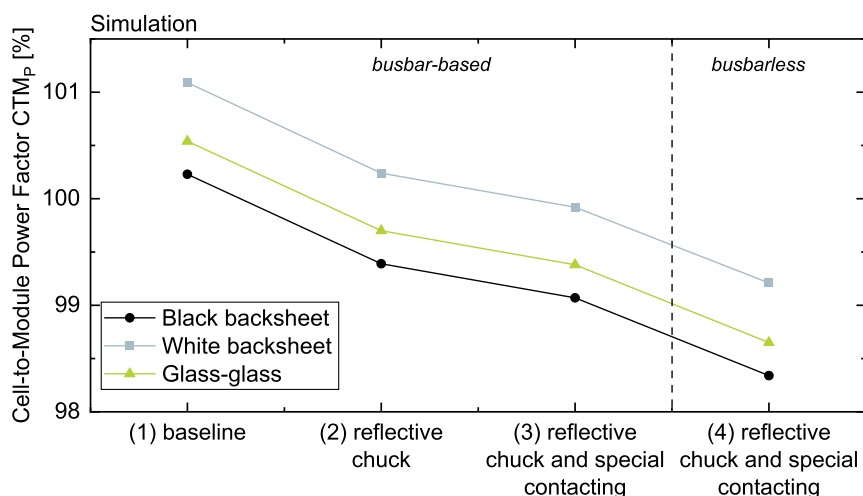


Figure 11. Simulated cell-to-module power factors CTM_P for the three module layouts as resulting from the corresponding solar cell measurement configurations. For purpose of clarity, only the PERC results are shown here.

For example, a black-backsheet module measured with the baseline configuration with nonreflective chuck yields comparable CTM_P factors as a white-backsheet module measured with the reflective-chuck configuration. This shows that there is not only a single most significant cell measurement configuration that can be universally applied for all module layouts, but that the optimal cell measurement configuration has to be evaluated for each module layout individually.

For meaningful cell measurement results, it seems reasonable to consider several issues. 1) busbar or interconnector shading should be taken into account to prevent underestimation of shading effects. 2) The reflectance of the measurement chuck should be adapted to the reflectance of the backsheet to correctly consider the bifaciality of the solar cells. 3) The front and rear contacting scheme should be adapted to the interconnection pattern of the module to correctly consider the series resistance of the finger grids of the solar cells.

It is in the scope of calibration laboratories to assist here by giving recommendations on how to calibrate reference cells to yield highest significance of cell measurements. If an adaption of the measurement configurations should not be possible, the effect of the measurement configurations on the solar cell parameters should be considered in CTM_P considerations.

5. Summary and Conclusions

In this article, the notation for solar cell measurement conditions which has recently been introduced to the Solar Cell Efficiency Tables has been examined in detail. It has been shown that different efficiency values can exist for the same solar cell because of different measurement conditions.

The effect of the measurement conditions on solar cell efficiency has been quantified based on simulations and measurements. It has been demonstrated that the application of a reflective chuck can lead to a difference in cell efficiency of 0.2–0.3%_{abs} for typical industrial PERC and TOPCon solar cells.

This difference is expected to increase further for lower solar cell thicknesses. Going to a busbarless solar cell design can even lead to efficiency differences of 0.5%_{abs}. The efficiency differences are mainly coming from optical effects, leading to increases in short-circuit current. The differences determined here must be considered as estimates as they can vary for different solar cell structures. The solar cells thus cannot be regarded as separate from the measurement system, but the measurement system needs to be considered and information on it needs to be reported together with the measurement results.

To evaluate the significance of the solar cell measurement conditions, the prediction of the module performance by solar cell measurements has been evaluated. By modeling the module integration of the solar cells, it has been shown that the power gains coming from different cell measurement configurations on solar cell level do not occur on the module level in the same manner. Higher measured solar cell efficiencies can thus lead to considerably reduced cell-to-module power factors. It is necessary to carefully choose the solar cell measurement conditions and to not only aim for highest measured efficiency values alone. Several hints to increase the significance of measurement conditions have been given.

The authors would like to emphasize that it is essential to include the solar cell measurement conditions in solar cell data sheets, in publications, and even press releases to allow for an objective assessment of the measurement results. Measurement values can only be evaluated correctly if the measurement conditions are given. Moreover, it is important that technology groups analyze their solar cell optimization routes carefully to avoid misdirected cell optimization caused by inappropriate measurement conditions. Finally, module manufacturers purchasing solar cells need to be aware that the power and efficiency of the solar cells used for manufacturing modules can potentially be under- or overrated.

Calibration laboratories always provide the measurement conditions and the relevant supplementary information, and it is important that this information is used and reported.

Acknowledgements

The authors would like to thank Pietro Altermatt for his great support in defining the solar cell simulation models.

Open Access funding enabled and organized by Projekt DEAL.

Conflict of Interest

The authors declare no conflict of interest.

Data Availability Statement

The data that support the findings of this study are available from the corresponding author upon reasonable request.

Keywords

current–voltage (*I*–*V*) measurements, measurement conditions, significance of measurements, silicon solar cells, solar cell efficiencies tables

Received: October 27, 2023

Revised: November 23, 2023

Published online: December 17, 2023

- [1] VDMA, *International Technology Roadmap for Photovoltaic (ITRPV): Results 2022*, 14th ed., **2023**, VDMA, Frankfurt am Main Germany.
- [2] C. N. Kruse, M. Wolf, C. Schinke, D. Hinken, R. Brendel, K. Bothe, *IEEE J. Photovoltaics* **2017**, 7, 747.
- [3] M. Rauer, A. Krieg, A. Fell, S. Pingel, N. Wöhrle, J. M. Greulich, S. Rein, M. C. Schubert, J. Hohl-Ebinger, *Sol. Energy Mater. Sol. Cells* **2022**, 248, 111988.
- [4] S. Raj, J. W. Ho, J. Wong, A. G. Aberle, *IEEE J. Photovoltaics* **2017**, 7, 1203.
- [5] J. Hohl-Ebinger, W. Warta, in *Proc. 25th European Photovoltaic Solar Energy Conf. Exhibition*, Valencia, Spain **2010**, p. 1358.
- [6] M. Rauer, K. Bothe, C. Comparotto, P. Danzl, M. Debucquoy, N. Enjalbert, J. Hohl-Ebinger, P. Manshanden, Y. Veschetti, J. Kai Chi Wong, in *Proc. 32nd European Photovoltaic Solar Energy Conf. Exhibition*, Munich, Germany **2016**, p. 915.
- [7] J. P. Singh, J. Chai, M. H. Saw, Y. S. Khoo, *Jpn. J. Appl. Phys.* **2017**, 56, 08MD04.
- [8] M. A. Green, E. D. Dunlop, J. Hohl-Ebinger, M. Yoshita, N. Kopidakis, K. Bothe, D. Hinken, M. Rauer, X. Hao, *Prog. Photovoltaics Res. Appl.* **2022**, 30, 687.
- [9] International Electrochemical Commission, IEC 60904-1, *Photovoltaic Devices – Part 1: Measurement of Photovoltaic Current-Voltage Characteristics* **2020**, IEC, Geneva, Switzerland.
- [10] International Electrochemical Commission, IEC 60904-1-2, *International Technical Specification. Version 1* **2019**, IEC, Geneva, Switzerland.
- [11] K. Bothe, C. Kruse, D. Hinken, M. Rauer, J. Hohl-Ebinger, R. Brendel, in *Proc. 37th European Photovoltaic Solar Energy Conf. Exhibition* **2020**, WIP Renewable Energies, Munich, Germany, pp. 277–281.
- [12] N. Bassi, C. Clerc, Y. Pelet, J. Hiller, V. Fakhfour, C. Droz, M. Despeisse, J. Levrat, A. Faes, D. Baetzner, P. Papet, in *Proc. 29th European Photovoltaic Solar Energy Conf. Exhibition*, Amsterdam, The Netherlands **2014**, p. 1180.
- [13] K. Ramspeck, P. Waleska, S. Schenk, M. Alt, R. Jakob, M. Meixner, in *Proc. 36th European Photovoltaic Solar Energy Conf. Exhibition*, Marseille, France **2019**, p. 443.
- [14] K. Kamatani, H. Kitamura, H. Kojima, Y. Nakamichi, Y. Fujita, K. Shibamoto, S. Kojima, in *Proc. 36th European Photovoltaic Solar Energy Conf. Exhibition* **2021**, WIP Renewable Energies, Munich, Germany, pp. 111–115.
- [15] R. C. Giri, D. Böhler, P. Breul, F. Schwindt, M. Neher, F. Steinert, *Property Organ* **2020**, <https://worldwide.espacenet.com/patent/search/family/075529976/publication/WO2021198259A1?q=WO2021198259A1>.
- [16] A. Fell, J. Schön, M. C. Schubert, S. W. Glunz, *Sol. Energy Mater. Sol. Cells* **2017**, 173, 128.
- [17] W. Wöhler, J. Greulich, *IEEE J. Photovoltaics*.
- [18] J. A. Rand, P. A. Basore, in *Proc. 22nd IEEE Photovoltaic Specialists Conf.*, Las Vegas **1991**, pp. 192–197.
- [19] A. Fell, J. Greulich, F. Feldmann, C. Messmer, J. Schön, M. Bivour, M. C. Schubert, S. W. Glunz, *Sol. Energy Mater. Sol. Cells* **2022**, 236, 111534.
- [20] R. Kopecek, J. Libal, *Photovoltaics Int.* **2021**, 47, 37.
- [21] I. Haedrich, U. Eitner, M. Wiese, H. Wirth, *Sol. Energy Mater. Sol. Cells* **2014**, 131, 14.
- [22] H. Hanifi, C. Pfau, D. Daßler, J. Schneider, S. Schindler, M. Turek, J. Bagdahn, *Photovoltaics Int.* **2016**, 32, 90.
- [23] M. Mittag, M. Ebert, *Photovoltaics Int.* **2017**, 36, 97.
- [24] Fraunhofer Institute for Solar Energy Systems ISE, www.cell-to-module.com (accessed: September 2023).
- [25] P. Papet, J. Levrat, N. Bassi, Y. Yao, A. Waltinger, V. Fakhfour, T. Soderstrom, B. Strahm, in *7th Metallization and Interconnection Workshop* **2017**.